

Chiral perturbation theory with vector mesons and the pion form factors

Tae-Sun Park

Center for Exotic Nuclear Studies, Institute for Basic Science, Daejeon 34126, Korea

Abstract

The chiral perturbation theory (ChPT) of pions is extended to include vector mesons as well as pertinent degrees of freedom. By counting the typical momentum scale of vector mesons as order of Q and vector meson masses as of order of Λ_χ , a consistent theory could be obtained. The explicit renormalization procedure of the theory is presented for the form factors of the pion up to one-loop accuracy. The resulting theory prediction for the form factors is in good agreement with the experimental data for a wide range of momentum transfers. The vector-meson dominance mechanism is also discussed in the systematic framework of ChPT.

Keywords: chiral perturbation theory, vector mesons, pion form factor

1. Introduction

Chiral perturbation theory (ChPT) [1, 2, 3, 4, 5] is a well-proven low-energy effective field theory (EFT) of QCD, and usually consists of only pions and nucleons (for the cases where $\Delta(1232)$ isobars are also included, see, for example, Refs. [6, 7, 8]). All other massive degrees of freedom are integrated out. Integrating out heavy fields is one of the key aspects that make ChPT a consistent and powerful expansion scheme with respect to powers of Q/Λ_χ , where Q stands for the typical momentum scale of the process and/or the pion mass, which is treated as “light” compared to the chiral scale $\Lambda_\chi \simeq 4\pi f_\pi \simeq 1$ GeV.

Promoting some of those integrated-out fields as pertinent degrees of freedom corresponds to a reassessment of a certain class of contributions, and

Email address: `tspark@ibs.re.kr` (Tae-Sun Park)

thus has the potential advantage of widening the validity region and increasing the accuracy of the theory. The inclusion of the Delta isobars, for example, is in line with this approach.

In this paper, limiting myself only to the meson sector in SU(2) for the sake of simplicity, ChPT is extended to include vector mesons that play important roles in nuclear physics [9, 10]. To this end, I adopt the power counting scheme where the typical momentum scale and the masses of vector mesons are counted as of order of Q and Λ_χ , respectively. The counter-term Lagrangian that absorbs all the divergences of the loop contributions up to the next-to-leading order (NLO) is identified, and the resulting theory is applied to the electric form factors of the pion up to NLO. It will be shown that the theory is in very good agreement with the experimental data up to $Q^2 \sim 1 \text{ GeV}^2$. The vector-meson dominance (VMD) mechanism [11, 12] will also be discussed in the framework of ChPT.

This manuscript is organized as follows. The formalism for the ChPT with vector mesons as well as pions is presented in the next section, where the counting rule and the Lagrangian up-to next-to-leading order Lagrangians are discussed. with A detailed the renormalization procedure for some relevant vertex functions is also presented in this section. In Sec. 3, the pion form factors up to one-loop accuracy are evaluated and compared with experimental data. Then a final summary is given in Sec. 4.

2. Formalism

2.1. Power counting rule and the Lagrangian

In this paper, since I am interested in the low-energy processes of pions where vector mesons appear only in intermediate states, it is natural to adopt the counting scheme where the typical scale of the momenta carried by the vector-mesons p is regarded in the order of Q , and the vector meson masses m_ρ in the order of Λ_χ . The corresponding counting rule has been discussed in Refs. [13, 14], where it is shown that a Feynman diagram characterized by the number E_H (E_e) of vector mesons (external gauge fields) and the number of L loops is of the order of Q^ν (modulo powers of f_π and Λ_χ) with

$$\nu = 2 - E_H - E_e + 2L + \sum_i \nu_i, \quad \nu_i \equiv d_i + h_i + e_i - 2, \quad (1)$$

where d_i , h_i and e_i are the number of derivatives and/or pion masses, vector mesons, and external gauge fields, respectively, attached to the i -th vertex.

And the leading-order (LO) Lagrangian consists of terms with $\nu_i = 0$,

$$\mathcal{L}_0 = \mathring{f}_\pi^2 \langle i\Delta_\mu i\Delta^\mu \rangle + \frac{1}{4} \mathring{f}_\pi^2 \langle \chi_+ \rangle + \mathring{a} \mathring{f}_\pi^2 \langle (g\rho_\mu - i\Gamma_\mu)^2 \rangle, \quad (2)$$

where $\rho_\mu \equiv \frac{1}{2} \tau^a \rho_\mu^a$ is the rho-meson field,

$$\begin{aligned} \Gamma_\mu + \Delta_\mu &= i\xi^\dagger \partial_\mu \xi + i\xi^\dagger (\mathcal{V}_\mu + \mathcal{A}_\mu) \xi, \\ \Gamma_\mu - \Delta_\mu &= i\xi \partial_\mu \xi^\dagger + i\xi (\mathcal{V}_\mu - \mathcal{A}_\mu) \xi^\dagger, \\ \chi_+ &= \xi^\dagger \chi \xi^\dagger + \xi \chi^\dagger \xi, \end{aligned} \quad (3)$$

\mathcal{V}_μ , \mathcal{A}_μ and χ are external fields: The vacuum expectation value of χ is \mathring{m}_π^2 , the *bare* mass of the pion squared, while others have vanishing vacuum expectation values. The bare quantities that should be distinguished from the physical values are denoted by the “o” marks. See Ref. [4] for a detailed explanation. Under the chiral $SU(N_f)_L \times SU(N_f)_R$ transformation, U transforms as $U \rightarrow g_R U g_L^\dagger$, N_f is the number of flavors, and g_L and g_R are elements of $SU(N)_L$ and $SU(N)_R$, respectively. And ξ defined as $U = \xi \cdot \xi$, and transforms non-linearly in terms of $h[g_R, g_L, U]$ defined by $\xi \rightarrow g_R \xi h^\dagger = h \xi g_L^\dagger$ [1, 2]. And the transformation of other quantities read $i\Delta_\mu \rightarrow h i\Delta_\mu h^\dagger$, $i\Gamma_\mu \rightarrow h i\Gamma_\mu h^\dagger - i\partial_\mu h h^\dagger$, and $g\rho_\mu \rightarrow h g\rho_\mu h^\dagger - i\partial_\mu h h^\dagger$. In the above equation, $\langle X \rangle$ stands for the trace of X in the isospin space, g is the rho-meson coupling constant, and the dimensionless parameter \mathring{a} is related to the rho meson mass, $m_\rho^2 = \mathring{a} g^2 \mathring{f}_\pi^2 + \mathcal{O}(Q^2)$.

One might be surprised to find that the LO Lagrangian does not contain the usual kinetic term for vector mesons, $\mathcal{L}_\rho^{\text{kin}} = -\frac{1}{2} \langle \rho^{\mu\nu} \rho_{\mu\nu} \rangle$, which appears only in the next-to-leading order (NLO) with $\nu_i = 2$ in this formalism. Without the kinetic term, the leading-order vector-meson propagator is momentum-independent, $\frac{1}{m_\rho^2} g^{\mu\nu} \delta^{ab}$. As a result, the rho-meson can be trivially integrated out at leading order, and the remaining theory becomes identical to the usual ChPT. However, at one-loop or higher-order calculations, the loop corrections cause the vector mesons introduced as pertinent degrees of freedom to play a non-trivial role.

There are different options for counting m_ρ and p . To describe the processes where rho mesons appear as external particles or those that involve momentum transfer whose size is comparable to m_ρ , Djukanovic et al. have developed a power counting scheme [15, 16] where the possible flows of the external momenta through the internal propagators are considered, assigning the chiral order of a Feynman diagram as the lowest among all the possible

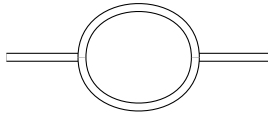


Figure 1: The most divergent one-loop diagram for the rho-meson self-energy. The double lines are rho-meson propagators.

cases. In this scheme, the rho-meson kinetic term enters in the leading order and the leading order rho-meson propagator is the familiar massive vector-meson propagator in the unitary gauge,

$$\frac{1}{k^2 - m_\rho^2 + i0^+} \left(-g_{\mu\nu} + \frac{k_\mu k_\nu}{m_\rho^2} \right) \delta^{ab}. \quad (4)$$

However, this propagator behaves poorly in the ultraviolet region. For example, the diagram given in Fig. 1 with this propagator results in a highly divergent term of the form $\frac{1}{d-4} k^4 (k^\mu k^\nu - g^{\mu\nu} k^2)$, where d is the space-time dimension.

This problem can be resolved if one adopts the so-called infrared regularization [17] or the extended-on-mass-shell scheme [18], where the contribution of the diagram vanishes identically. Another possibility is to adopt the hidden local gauge symmetry (HLS) where the rho meson is introduced as a gauge boson of the *hidden* symmetry [19, 20]. In HLS, one can adopt a general R_ξ gauge propagator, which removes the aforementioned problem. One-loop calculations in HLS come with however its own complications related to the gauge-fixing of the hidden symmetry. For a comprehensive discussion of one-loop calculation in HLS in the chiral limit, see Ref. [20].

The formalism presented in this paper is free from the above-mentioned divergence, since there is no $\rho\rho\rho$ -vertex at LO and thus the aforementioned problematic one-loop diagram does not appear.

2.2. 1-loop divergences

In Refs. [3, 4], the 1-loop contributions to the vacuum functional is evaluated for the chiral perturbation theory with pions. By applying the same procedure to the cases where vector mesons are also included, one can identify the counter-term Lagrangian that absorbs all the divergences of the one-loop

graphs with the LO Lagrangian,

$$\begin{aligned}
\mathcal{L}_{ct} = & \frac{1}{16\pi^2(d-4)} \left\{ \frac{N}{6} \langle \tilde{\Gamma}_{\mu\nu} \tilde{\Gamma}^{\mu\nu} \rangle \right. \\
& + 2 \langle \Delta^\mu \Delta^\nu \rangle \langle \Delta_\mu \Delta_\nu \rangle - \mathring{a}^2 \langle \Delta^\mu \phi^\nu \rangle \langle \Delta_\mu \phi_\nu \rangle \\
& + \frac{\mathring{a}^4}{8} \langle \phi^\mu \phi^\nu \rangle \langle \phi_\mu \phi_\nu \rangle \\
& + \langle W \rangle^2 + N \langle W^2 \rangle - \frac{N}{2} \langle \chi_+ W \rangle - \frac{1}{2} \langle \chi_+ \rangle \langle W \rangle \\
& + \frac{N^2 - 4}{16N} \langle \chi_+^2 \rangle + \frac{N^2 + 2}{16N^2} \langle \chi_+ \rangle^2 \left. \vphantom{\frac{1}{16\pi^2(d-4)}} \right\} \\
& + \cdots,
\end{aligned} \tag{5}$$

where the ellipses denote non-divergent terms, N is the flavor number ($N = 2$ in this work), $\phi_\mu \equiv (g\rho_\mu - i\Gamma_\mu)$, $W \equiv \Delta^\mu \Delta_\mu - \frac{\mathring{a}^2}{4} \phi^\mu \phi_\mu$, and

$$\begin{aligned}
\tilde{\Gamma}_{\mu\nu} = & \left(1 - \frac{\mathring{a}}{2} \right) \Gamma_{\mu\nu} - i \frac{\mathring{a}}{2} g \rho_{\mu\nu} \\
& + \frac{\mathring{a}}{2} \left(1 - \frac{\mathring{a}}{2} \right) [g\rho_\mu - i\Gamma_\mu, g\rho_\nu - i\Gamma_\nu]
\end{aligned} \tag{6}$$

with $\Gamma_{\mu\nu} \equiv \partial_\mu \Gamma_\nu - \partial_\nu \Gamma_\mu + [\Gamma_\mu, \Gamma_\nu]$ and $\rho_{\mu\nu} \equiv \partial_\mu \rho_\nu - \partial_\nu \rho_\mu - ig [\rho_\mu, \rho_\nu]$.

2.3. Renormalization of vertex functions

The renormalization procedure of the vertex functions that are relevant for the electromagnetic form factors of the pion is described here. The relevant Lagrangian may be written as

$$\begin{aligned}
\mathcal{L}_2 = & -\frac{1}{2} C_{1:1} g^2 \langle \rho_{\mu\nu} \rho^{\mu\nu} \rangle + \frac{1}{2} C_{1:2} \langle \Gamma_{\mu\nu} \Gamma^{\mu\nu} \rangle \\
& - i C_{1:3} g \langle \rho^{\mu\nu} \Gamma_{\mu\nu} \rangle \\
& - i C_{2:1} g \langle \rho_{\mu\nu} [\Delta^\mu, \Delta^\nu] \rangle + C_{2:2} \langle \Gamma_{\mu\nu} [\Delta^\mu, \Delta^\nu] \rangle \\
& - C_3 \langle \chi_+ \rangle \langle \Delta^\mu \Delta_\mu \rangle + C_4 \langle \chi_+ \rangle \langle (g\rho_\mu - i\Gamma_\mu)^2 \rangle \\
& + C_5 \langle \chi_+ \rangle^2 + \cdots,
\end{aligned} \tag{7}$$

where the ellipses represent terms that contain four or more fields. I adopt the convention of Refs. [3, 4] which decompose the low-energy constants (LECs)

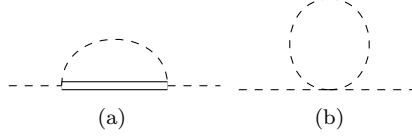


Figure 2: 1PI diagrams for $\pi_a(k) \rightarrow \pi_b(k)$. The dashed lines denote pions.

into a divergent part and the remaining finite part,

$$C_i = \eta_i \left[\lambda + \frac{1}{32\pi^2} \left(\bar{C}_i + \ln \frac{\dot{m}_\pi^2}{\mu^2} \right) \right], \quad (8)$$

where μ is the scale of the dimensional regularization, and

$$\lambda \equiv -\frac{\mu^{d-4}}{32\pi^2} \left\{ \frac{2}{4-d} + \ln 4\pi + \Gamma'(1) + 1 \right\}. \quad (9)$$

The renormalized \bar{C}_i are independent of the scale μ , and the coefficient η_i can

be obtained by comparing Eq.(7) with (5): $\{\eta_{1:1}, \eta_{1:2}, \eta_{1:3}\} = \frac{2}{3} \left\{ \frac{\ddot{a}^2}{4}, \left(1 - \frac{\ddot{a}}{2}\right)^2, \frac{\ddot{a}}{2} \left(1 - \frac{\ddot{a}}{2}\right) \right\}$,
 $\eta_{2:1} = \eta_{2:2} = 0$, $\{\eta_3, \eta_4\} = \left\{ 1, \frac{\ddot{a}^2}{4} \right\}$ and $\eta_5 = \frac{3}{32}$.

2.3.1. 1PI for $\pi_a(k) \rightarrow \pi_b(k)$

The one-particle irreducible (1PI) vertex for $\pi_a(k) \rightarrow \pi_b(k)$ is the inverse of the pion propagator $\delta_{ab} D_\pi(k^2)$, whose one-loop diagrams are drawn in Fig. 2. Their contributions are

$$\begin{aligned} D_\pi^{-1,(a)}(k^2) &= 2\ddot{a}k^2 \frac{\lambda_2}{f_\pi^2}, \\ D_\pi^{-1,(b)}(k^2) &= \left[2(1 - \ddot{a})k^2 - \frac{3}{2}\dot{m}_\pi^2 \right] \frac{\lambda_2}{f_\pi^2}, \end{aligned} \quad (10)$$

where

$$\lambda_2 \equiv -2\dot{m}_\pi^2 \left(\lambda + \frac{1}{32\pi^2} \ln \frac{\dot{m}_\pi^2}{\mu^2} \right). \quad (11)$$

There are also *tree* contributions from \mathcal{L}_0 and \mathcal{L}_2 ,

$$\begin{aligned} D_\pi^{-1,\text{tree}}(t) &= \frac{t}{f_\pi^2} \left(\dot{f}_\pi^2 + 4\dot{m}_\pi^2 C_3 \right) - \frac{\dot{m}_\pi^2}{f_\pi^2} \left(\dot{f}_\pi^2 + 32\dot{m}_\pi^2 C_5 \right) \\ &\equiv (1 + \delta Z_\pi)t - (m_\pi^2 + \delta m_\pi^2), \end{aligned} \quad (12)$$

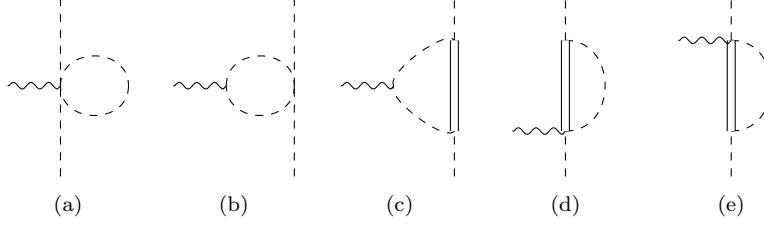


Figure 3: 1PI diagrams for $\mathcal{V}_e^\mu(k) \rightarrow \pi_a(q_a) + \pi_b(q_b)$. The wiggled lines denote external vector fields.

which defines δZ_π and δm_π^2 . The net sum then reads

$$\begin{aligned} D_\pi^{-1}(t) &\equiv D_\pi^{-1,(a)}(t) + D_\pi^{-1,(b)}(t) + D_\pi^{-1,\text{tree}}(t) \\ &= t - m_\pi^2 \end{aligned} \quad (13)$$

with

$$\begin{aligned} \delta Z_\pi &= -2 \frac{\lambda_2}{f_\pi^2}, \\ \delta m_\pi^2 &= -\frac{3}{2} \frac{\lambda_2}{f_\pi^2} \mathring{m}_\pi^2. \end{aligned} \quad (14)$$

Combining Eq.(12) with (14), one can express f_π and m_π in terms of the bare quantities,

$$\begin{aligned} f_\pi^2 &= \mathring{f}_\pi^2 + \frac{\mathring{m}_\pi^2}{8\pi^2} \bar{C}_3, \\ m_\pi^2 &= \mathring{m}_\pi^2 - \frac{\mathring{m}_\pi^4}{32\pi^2 f_\pi^2} (4\bar{C}_3 - 3\bar{C}_5). \end{aligned} \quad (15)$$

This is consistent with the results given in Ref.[3], which can be seen as C_3 and C_5 correspond to $\frac{1}{2}l_4$ and $\frac{1}{16}(l_3 + l_4)$, respectively.

The 1PI functions for $\pi_b(k) \rightarrow \mathcal{A}_a^\mu(k)$ and $\mathcal{A}_a^\mu(k) \rightarrow \mathcal{A}_b^\nu(k)$ can be evaluated in a similar way:

$$\Gamma[\pi_a(k) \rightarrow \mathcal{A}_b^\mu(k)] = ik^\mu f_\pi \delta_{ab}, \quad (16)$$

$$\Gamma[\mathcal{A}_a^\mu(k) \rightarrow \mathcal{A}_b^\nu(k)] = f_\pi^2 g^{\mu\nu} \delta_{ab}. \quad (17)$$

2.3.2. 1PI for $\mathcal{V}_e^\mu(k) \rightarrow \pi_a(q_a) + \pi_b(q_b)$

The 1PI diagrams for $\mathcal{V}_e^\mu(k) \rightarrow \pi_a(q_a) + \pi_b(q_b)$ are drawn in Fig. 3, and the corresponding vertex function can be written as $-i\epsilon_{eab}(q_a - q_b)^\mu \Gamma_{\mathcal{V}\pi\pi}(k^2)$ with

$$\begin{aligned}
\Gamma_{\mathcal{V}\pi\pi}^{(a)}(t) &= 3(1 - \mathring{a}) \frac{\lambda_2}{f_\pi^2}, \\
\Gamma_{\mathcal{V}\pi\pi}^{(b)}(t) &= -\frac{(2 - \mathring{a})^2}{4f_\pi^2} [\lambda_2 - t f_3(t)], \\
\Gamma_{\mathcal{V}\pi\pi}^{(c)}(t) &= 0, \\
\Gamma_{\mathcal{V}\pi\pi}^{(d+e)}(t) &= 2\mathring{a} \frac{\lambda_2}{f_\pi^2}, \\
\Gamma_{\mathcal{V}\pi\pi}^{\text{tree}}(t) &= 1 + \delta Z_\pi - \frac{1}{2f_\pi^2} \left(\mathring{a} f_\pi^2 + 4\mathring{m}_\pi^2 C_4 \right) \\
&\quad + \frac{t}{2f_\pi^2} (C_{1:2} - C_{2:2}), \tag{18}
\end{aligned}$$

where the loop function $f_3(t)$ is described in the Appendix A.

The net contribution is given as

$$\begin{aligned}
\Gamma_{\mathcal{V}\pi\pi}(t) &= 1 - \frac{a_r}{2} \\
&\quad + \frac{t}{2f_\pi^2} \left[2 \left(1 - \frac{\mathring{a}}{2} \right)^2 f_3(t) + C_{1:2} - C_{2:2} \right] \tag{19}
\end{aligned}$$

with

$$a_r = \mathring{a} - \frac{m_\pi^2}{8\pi^2} \left(\mathring{a} \bar{C}_3 - \frac{\mathring{a}^2}{4} \bar{C}_4 \right). \tag{20}$$

If $\mathring{a} = 0$, the results become identical to the ChPT without vector mesons. On the other hand, $a_r = 2$ (with $\mathring{a} = 2 + \mathcal{O}(Q^2/\Lambda_\chi^2)$) leads to a considerable amount of simplification. With this choice, for example, $\Gamma_{\mathcal{V}\pi\pi}(0) = 1 - \frac{a_r}{2}$ vanishes, and the photon coupling to the pion is mediated only by the 1ρ -exchange diagram drawn in Fig. 6(b), which is known as the vector-meson dominance (VMD) mechanism [11, 12]. $C_{1:2}$ is in general divergent and to be adjusted to absorb the divergence coming from $f_3(0)$. When $a_r = 2$, however, the loop contribution vanishes and $C_{1:2}$ becomes finite. The renormalization procedure for the linear combination $C_{1:2} - C_{2:2}$ will be discussed in Section 3.

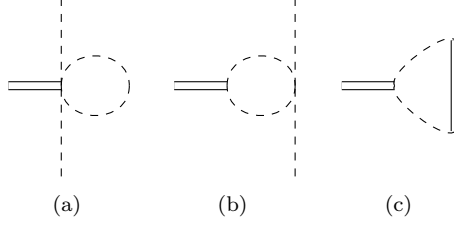


Figure 4: 1PI diagrams for $\rho_e^\mu(k) \rightarrow \pi_a(q_a) + \pi_b(q_b)$.

2.3.3. 1PI for $\rho_e^\mu(k) \rightarrow \pi_a(q_a) + \pi_b(q_b)$

The 1PI diagrams for $\rho_e^\mu(k) \rightarrow \pi_a(q_a) + \pi_b(q_b)$ are drawn in Fig. 4, whose vertex function can be written as $-i\epsilon_{cab}(q_a - q_b)^\mu \Gamma_{\rho\pi\pi}(k^2)$ with

$$\begin{aligned}
\Gamma_{\rho\pi\pi}^{(a)} &= \frac{\mathring{a}g}{2f_\pi^2} \lambda_2, \\
\Gamma_{\rho\pi\pi}^{(b)} &= \left(1 - \frac{\mathring{a}}{2}\right) \frac{\mathring{a}g}{2f_\pi^2} [-\lambda_2 + t f_3(t)], \\
\Gamma_{\rho\pi\pi}^{(c)} &= 0, \\
\Gamma_{\rho\pi\pi}^{\text{tree}} &= \frac{g}{2f_\pi^2} \left\{ \mathring{a} \mathring{f}_\pi^2 + 4\mathring{m}_\pi^2 C_4 + (C_{1:3} - C_{2:1}) t \right\},
\end{aligned} \tag{21}$$

and the net sum reads

$$\Gamma_{\rho\pi\pi}(t) = \frac{a_r}{2} g + \frac{g}{2f_\pi^2} t \left[\mathring{a} \left(1 - \frac{\mathring{a}}{2}\right) f_3(t) + C_{1:3} - C_{2:1} \right]. \tag{22}$$

When $a_r = 2$, the loop contribution vanishes and one is left with

$$\Gamma_{\rho\pi\pi}(t)|_{a_r=2} = g + \frac{t}{m_\rho^2} (g_{\rho\pi\pi} - g), \tag{23}$$

where

$$g_{\rho\pi\pi} \equiv \Gamma_{\rho\pi\pi}(m_\rho^2) = g \left[1 + \frac{m_\rho^2}{2f_\pi^2} (C_{1:3} - C_{2:1}) \right] \tag{24}$$

is to be determined. Since $\Gamma(\rho^0 \rightarrow \pi^+\pi^-) = g_{\rho\pi\pi}^2 p_\pi^3 / (6\pi m_\rho^2)$ with $p_\pi \equiv \sqrt{m_\rho^2/4 - m_\pi^2}$, the experimental data for the rho meson decay width $\Gamma(\rho^0 \rightarrow \pi^+\pi^-) = (147.8 \pm 0.9)$ MeV corresponds to

$$g_{\rho\pi\pi} = 5.942 \pm 0.017. \tag{25}$$

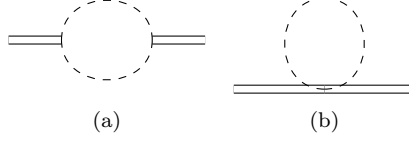


Figure 5: 1PI diagrams for $\rho_a^\mu(k) \rightarrow \rho_b^\nu(k)$.

2.3.4. 1PI for $\rho_a^\mu(k) \rightarrow \rho_b^\nu(k)$

The vertex function for $\rho_a^\mu(k) \rightarrow \rho_b^\nu(k)$ is the inverse of the rho-meson propagator $\delta_{ab}D_\rho^{\mu\nu}(k)$, whose relevant diagrams are drawn in Fig. 5:

$$\begin{aligned}
(D_\rho^{-1})^{\mu\nu,(a)}(k) &= \frac{1}{2}\mathring{a}^2 g^2 \lambda_2 g^{\mu\nu} \\
&\quad + \frac{1}{2}\mathring{a}^2 g^2 (k^\mu k^\nu - g^{\mu\nu} k^2) f_3(k^2), \\
(D_\rho^{-1})^{\mu\nu,(b)}(k) &= 0, \\
(D_\rho^{-1})^{\mu\nu,\text{tree}}(k) &= g^2 \left(\mathring{a} f_\pi^2 + 4\mathring{m}_\pi^2 C_4 \right) g^{\mu\nu} \\
&\quad + g^2 C_{1:1} (k^\mu k^\nu - g^{\mu\nu} k^2),
\end{aligned} \tag{26}$$

and the resulting propagator is given as

$$D_\rho^{\mu\nu}(k) = -D_\rho(k^2) \left(g^{\mu\nu} - A_\rho(k^2) \frac{k^\mu k^\nu}{a_r g^2 f_\pi^2} \right) \tag{27}$$

with

$$D_\rho(t) = [t A_\rho(t) - a_r g^2 f_\pi^2]^{-1}, \tag{28}$$

$$A_\rho(t) = g^2 C_{1:1} + \frac{1}{2}\mathring{a}^2 g^2 f_3(t). \tag{29}$$

The renormalization condition for g and $C_{1:1}$ may be obtained by demanding the following structure of the propagator near the pole position,

$$\lim_{t \rightarrow m_\rho^2} D_\rho^{-1}(t) = t - m_\rho^2 + i m_\rho \Gamma_\rho, \tag{30}$$

where $\Gamma_\rho \simeq \Gamma(\rho^0 \rightarrow \pi^+ \pi^-)$ is the decay width of the rho meson. In this work, to reproduce the imaginary part of the above equation accurately, $\bar{A}_\rho(t) \equiv A_\rho(t) - A_\rho(0)$ is rewritten as

$$\bar{A}_\rho(t) = 2 [\Gamma_{\rho\pi\pi}(t)]^2 \bar{f}_3(t), \tag{31}$$

where the tree order $\rho\pi\pi$ coupling $\frac{a_r}{2}g$ is replaced by the full one-loop order vertex function $\Gamma_{\rho\pi\pi}(t)$. Since $\Gamma_{\rho\pi\pi}(t) = \frac{a_r}{2}g + \mathcal{O}(Q^2/\Lambda_\chi^2)$ when $t = \mathcal{O}(Q^2)$, this replacement is correct up to one-loop accuracy, but contains the higher-order contributions needed to reproduce the experimental ρ -meson decay width at the pole position. Then the solution for $a_r g^2 f_\pi^2 = t \Re A_\rho(t)$ and $\frac{\partial}{\partial t} (t \Re A_\rho(t)) = 1$ at $t = m_\rho^2$ reads¹

$$\begin{aligned} g &= \frac{m_\rho}{\sqrt{a_r} f_\pi} \left[\frac{\sqrt{a_r} g_{\rho\pi\pi} m_\rho}{f_\pi} R_3 \right. \\ &\quad \left. + \sqrt{1 - 2g_{\rho\pi\pi}^2 (2R_3 + m_\rho^2 R'_3)} \right] \\ &\simeq 6.21 \pm 0.06, \\ A_\rho(0) &= \frac{a_r g^2 f_\pi^2}{m_\rho^2} - 2g_{\rho\pi\pi}^2 R_3 \simeq 1.113 \pm 0.002, \end{aligned} \quad (33)$$

where $R_3 \equiv \Re \bar{f}_3(m_\rho^2) \simeq -0.3395 \times 10^{-3}$, $R'_3 \equiv \Re f'_3(m_\rho^2) \simeq -1.289 \times 10^{-3}/m_\rho^2$ and $f'_3(t) \equiv \frac{\partial}{\partial t} f_3(t)$, with $a_r = 2$, $m_\rho = (775.26 \pm 0.23)$ MeV and $f_\pi = (92.1 \pm 0.8)$ MeV [21].

The low-momentum behavior of the propagator is given as

$$\lim_{k^2 \rightarrow 0} D_\rho^{\mu\nu}(k) = \frac{1}{A_\rho(0)} \frac{1}{\tilde{M}_\rho^2 - k^2} \left(g^{\mu\nu} - \frac{k^\mu k^\nu}{\tilde{M}_\rho^2} \right), \quad (34)$$

where

$$\tilde{M}_\rho \equiv \frac{\sqrt{a_r} g f_\pi}{\sqrt{A_\rho(0)}} \simeq (0.989 \pm 0.001) m_\rho. \quad (35)$$

Thus, its overall magnitude is quenched by the factor $1/A_\rho(0) \simeq 0.90$, with an “effective mass” which is about 1 percent smaller than physical mass, $\tilde{M}_\rho \simeq 0.99 m_\rho$.

¹If one does not invoke the replacement given in Eq.(31), the corresponding solution would be

$$\begin{aligned} g &= \left(\frac{a_r f_\pi^2}{m_\rho^2} + \frac{1}{2} a_r^2 m_\rho^2 R'_3 \right)^{-1/2} \simeq 6.25 \pm 0.06, \\ A_\rho(0) &= \frac{a_r g^2 f_\pi^2}{m_\rho^2} - \frac{1}{2} a_r^2 g^2 R_3 \simeq 1.125 \pm 0.035. \end{aligned} \quad (32)$$

Similarly, the 1PI for $\rho_a^\mu(k) \rightarrow \mathcal{V}_b^\nu(k) \equiv \Gamma_{\rho\mathcal{V}}^{\mu\nu}(k)$ reads

$$\begin{aligned}\Gamma_{\rho\mathcal{V}}^{\mu\nu}(k) &= -\Gamma_{\rho\mathcal{V}}(k^2)g^{\mu\nu} \\ &+ g \left[\dot{a} \left(1 - \frac{\dot{a}}{2} \right) f_3(k^2) + C_{1:3} \right] k^\mu k^\nu\end{aligned}\quad (36)$$

with

$$\Gamma_{\rho\mathcal{V}}(t) = a_r g f_\pi^2 + g \left[\dot{a} \left(1 - \frac{\dot{a}}{2} \right) f_3(t) + C_{1:3} \right] t. \quad (37)$$

$\Gamma_{\rho\mathcal{V}}(m_\rho^2)$ is related to the $\rho \rightarrow e^+e^-$ decay width as

$$\Gamma(\rho \rightarrow e^+e^-) = \frac{8\pi\alpha^2}{3m_\rho^4} |\Gamma_{\rho\mathcal{V}}(m_\rho^2)|^2 \left(1 + 2\frac{m_e^2}{m_\rho^2} \right) p_e$$

with $p_e \equiv \sqrt{m_\rho^2/4 - m_e^2}$. The experimental value $\Gamma(\rho \rightarrow e^+e^-) = (7.04 \pm 0.06)$ keV corresponds to

$$\Gamma_{\rho\mathcal{V}}(m_\rho^2) = (0.1213 \pm 0.0005) \text{ GeV}^2 \quad (38)$$

and

$$\frac{\Gamma_{\rho\mathcal{V}}(m_\rho^2)}{2f_\pi^2 g_{\rho\pi\pi}} = 1.197 \pm 0.006. \quad (39)$$

The values of $C_{1:3}$ and $C_{2:1}$ that reproduce the experimental values for $\Gamma(\rho \rightarrow \pi^+\pi^-)$ and $\Gamma(\rho \rightarrow e^+e^-)$ can be obtained by combining Eqs.(24,25,37,38), for the particular choice $a_r = 2$,

$$\begin{aligned}C_{1:3} &= (4.3 \pm 1.0) \times 10^{-3}, \\ C_{2:1} &= (5.5 \pm 0.7) \times 10^{-3}.\end{aligned}\quad (40)$$

3. Electric form factors of the pion

The electric form factor of the pion, $F_\pi(t)$, is the sum of the 1PI $\mathcal{V}\pi\pi$ vertex and the one ρ -meson-exchange,

$$\begin{aligned}F_\pi(t) &= \Gamma_{\mathcal{V}\pi\pi}(t) \\ &+ \frac{a_r g^2 f_\pi^2}{a_r g^2 f_\pi^2 - t A_\rho(t)} \frac{\Gamma_{\rho\pi\pi}(t)}{\Gamma_{\rho\pi\pi}(0)} \frac{\Gamma_{\rho\mathcal{V}}(t)}{\Gamma_{\rho\mathcal{V}}(0)}.\end{aligned}\quad (41)$$

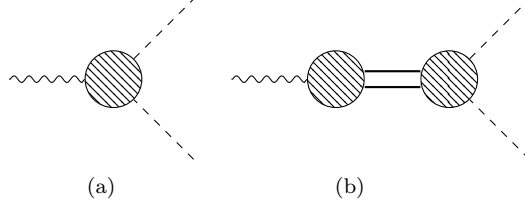


Figure 6: Diagrams for the electric form factor of the pion.

$F_\pi(t)$ at small- t is given as $F_\pi(t) = 1 + \frac{1}{6}\langle r_\pi^2 \rangle t + \mathcal{O}(t^2)$ with

$$\frac{1}{6}\langle r_\pi^2 \rangle = \Gamma'_{\mathcal{V}\pi\pi}(0) + \frac{1}{\tilde{M}_\rho^2} + \frac{1}{2f_\pi^2} (2C_{1:3} - C_{2:1}), \quad (42)$$

where $\langle r_\pi^2 \rangle$ is the square of the charge radius of the pion. The experimental value $\langle r_\pi^2 \rangle = (0.434 \pm 0.005) \text{ fm}^2$ [21] with the values of $C_{1:3}$ and $C_{2:1}$ given in Eq.(40) leads to

$$\begin{aligned} \Gamma_{\mathcal{V}\pi\pi}(t) &= \Gamma'_{\mathcal{V}\pi\pi}(0) t, \\ \Gamma'_{\mathcal{V}\pi\pi}(0) &= \frac{C_{1:2} - C_{2:2}}{2f_\pi^2} = (0.000 \pm 0.005) \text{ fm}^2. \end{aligned} \quad (43)$$

That is, with $a_r = 2$, one has the complete VMD where not only the leading tree contribution but also the one-loop correction vanish for $\Gamma_{\mathcal{V}\pi\pi}(t)$, and the pion form factor is completely mediated by the vector-meson exchange.

The resulting $|F_\pi(t)|$ with $a_r = 2$ is drawn in the top panel of Fig. 7, which shows that the theory prediction is in excellent agreement with the experimental data [22].

This success comes as a surprise because the validity region of the formalism is limited to the low-energy region $Q < \Lambda_\chi$ and fitting to data was not required, the LECs have been fixed just to reproduce the experimental data for the charge radius of the pion and the $\rho \rightarrow \pi\pi$ and $\rho \rightarrow e^+e^-$ decay widths while adopting the choice $a_r = 2$.

3.1. $\rho - \omega$ mixing

Contrary to the pion form factor extracted from the $\tau^- \rightarrow \pi^- \pi^0 \nu_\tau$ decay that has been discussed so far, the form factor obtained from $\sigma(e^+e^- \rightarrow \pi^+\pi^-)$ [23, 24] is subject to the $\rho - \omega$ mixing [26, 27, 16]. As discussed in Refs. [25, 27], the effect of the mixing to the pion form factor is to multiply the

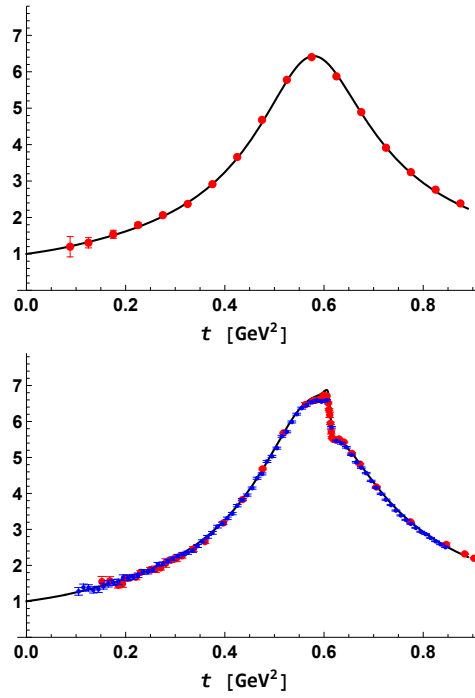


Figure 7: The electric form factors of the pion, $|F_\pi(t)|$, for the experimental data extracted from the $\tau^- \rightarrow \pi^- \pi^0 \nu_\tau$ decay [22] (top) and from the $e^+ e^- \rightarrow \pi^+ \pi^-$ cross-section [23, 24] (bottom). The black solid lines represent the theory prediction. In the bottom panel, the blue dots are for the KLOE data [23] while the red dots are for the SND data [24].

following factor to the rho-meson propagator (or, identically, to the second term of the pion form factor given in Eq.(41)),

$$1 + \frac{F_\omega}{F_\rho} \frac{\Theta_{\rho\omega}}{t - m_\omega^2 + im_\omega\Gamma_\omega}, \quad (44)$$

where, in the vicinity of $\rho - \omega$ resonance, $\Theta_{\rho\omega} = 2m_\rho(m_u - m_d) + e^2 F_\rho F_\omega$, and the vector meson coupling strengths are defined as $\langle 0 | j_\mu^{\text{em}} | \rho^0 \rangle = \varepsilon_\mu F_\rho m_\rho$ and $\langle 0 | j_\mu^{\text{em}} | \omega \rangle = \varepsilon_\mu F_\omega m_\omega$, ε_μ representing the polarization vector. With the values estimated in [27], $F_\omega/F_\rho = \frac{1}{3}$, $\Theta_{\rho\omega} = (-3.91 \pm 0.30) \times 10^{-3} \text{ GeV}^2$, and with the experimental value [21] $m_\omega = 782.66 \text{ MeV}$ and $\Gamma_\omega = 8.68 \text{ MeV}$, the resulting pion form factor is drawn in the bottom panel of Fig. 7.

4. Summary

In this work, the chiral perturbation theory of pions has been extended to include vector mesons as well. The employed power counting scheme is to count the masses and the momentum scale of the vector mesons as $\mathcal{O}(\Lambda_\chi)$ and $\mathcal{O}(Q)$, respectively. Up to one-loop accuracy, all the divergences have been identified, and the renormalization procedure for the vector form factor of the pion has been explicitly demonstrated. For the parameter a_r , the special choice $a_r = 2$ has been adopted as it simplifies the theory substantially. Interestingly, the theory with $a_r = 2$ retains the VMD mechanism even at one-loop accuracy. Thus one is left with $\Gamma_{\nu\pi\pi}(t) = 0$, and photons interact with pions only through vector-meson exchanges.

One-loop order calculations with vector mesons for the pion form factors are found to be in excellent agreement with the experimental data for a wide range of momentum transfers. However, this success should be taken with caution, as the general validity domain of the theory remains $Q \ll \Lambda_\chi \sim 1 \text{ GeV}$.

Acknowledgement

The author thanks Prof. S.-W. Hong and Prof. A.W. Thomas for useful discussions and their support. He is also grateful to Dr. Joohun (Jason) Park for his careful reading of the manuscript and helpful comments. This work was supported by the IBS grant funded by the Korea government (No. IBS-R031-D1).

Appendix A. Loop function

The loop function $f_3(k^2)$ is defined as [13],

$$f_3(k^2) = \frac{\Gamma(\varepsilon)}{16\pi^2} \int_0^1 dz z(2z-1) \left(\frac{m_\pi^2 - z(1-z)k^2}{4\pi\mu^2} \right)^{-\varepsilon}.$$

At $k^2 = 0$, it is given as with

$$f_3(0) = \frac{\lambda_0}{6} = -\frac{1}{6} \left[2\lambda + \frac{1}{16\pi^2} \left(\ln \frac{M^2}{\mu^2} - 1 \right) \right], \quad (\text{A.1})$$

and $\bar{f}_3(k^2) \equiv f_3(k^2) - f_3(0)$ reads

$$\begin{aligned} \bar{f}_3(k^2) &= \frac{1}{16\pi^2} \int_{2m_\pi}^\infty dM \frac{1}{3M} \left(1 - \frac{4m_\pi^2}{M^2} \right)^{3/2} \\ &\quad \times \frac{k^2}{M^2 - k^2(1-y^2)/4 - i0} \\ &= \frac{1}{16\pi^2} \left[\frac{1}{9} + \frac{1}{3\sigma^3} (\arctan \sigma - \sigma) \right], \end{aligned} \quad (\text{A.2})$$

$\sigma \equiv k/\sqrt{4m_\pi^2 - k^2 - i0}$. Its imaginary part reads

$$\Im f_3(k^2) = \frac{1}{96\pi} \left(\frac{k^2 - 4m_\pi^2}{k^2} \right)^{3/2} \theta(k - 2m_\pi), \quad (\text{A.3})$$

and $\bar{f}_3(m_\rho^2) = (-0.340 + 2.692i) \times 10^{-3}$ and $m_\rho^2 f'_3(m_\rho^2) = (-1.289 + 0.602i) \times 10^{-3}$.

References

- [1] S. Weinberg, Phys. Rev. 166, 1568 (1968).
- [2] S. Coleman, J. Wess and B. Zumino, Phys. Rev. 177 (1969) 2239;
C. Callan, S. Coleman, J. Wess and B. Zumino, Phys. Rev. 177 (1969) 2247.
- [3] J. Gasser and H. Leutwyler, “Chiral perturbation theory to one-loop”,
Ann. of Phys. 158 (1984) 142.

- [4] J. Gasser and H. Leutwyler, “Chiral perturbation theory: Expansions in the mass of the strange quark”, Nucl. Phys. B250 (1985) 465.
- [5] S. Weinberg, Phys. Lett. B251(1990) 288; Nucl. Phys. B363 (1991) 3.
- [6] H. Krebs, E. Epelbaum and U.-G. Meißner, Eur. Phys. J. A32 (2007) 127.
- [7] W.G. Jiang, A. Ekström, C. Forssén, G. Hagen, G. R. Jansen, and T. Papenbrock, Phys. Rev. C102 (2020) 054301.
- [8] Y. Nosyk, D.R. Entem and R. Machleidt, Phys. Rev. C104 (2021) 054001.
- [9] G.Ecker, J. Gasser, A. Pich and E.De Rafael, Nucl. Phys. B321 (1989) 311.
- [10] G.Ecker, J. Gasser, H. Leutwyler, A. Pich and E.De Rafael, Phys. Lett. B223 (1989) 425.
- [11] M. Gell-Mann and F. Zachariasen, Phys. Rev. 124 (1961) 953.
- [12] J.J. Sakurai, Currents and mesons (University of Chicago Press, Chicago, IL, 1969).
- [13] T.-S. Park, D.-P. Min and M. Rho, Phys. Repts. 233 (1995) 341.
- [14] M. Rho, Phys. Rev. Lett. 66 (1991) 1275.
- [15] D. Djukanovic, J. Gegelia, A. Keller, S. Scherer, Phys. Lett. B 680 (2009) 235.
- [16] D. Djukanovic, J. Gegelia, A. Keller, S. Scherer, and L. Tiator, Phys. Lett. B 742 (2015) 55.
- [17] T. Becher and H. Leutwyler, Eur. Phys. J. C9 (1999) 643.
- [18] T. Fuchs, J. Gegelia, G. Japaridze, and S. Scherer, Phys. Rev. D68 (2003) 056005.
- [19] M. Bando, T. Kugo, S. Uehara, K. Yamawaki, T. Yanagida, Phys. Rev. Lett. 54 (1985) 1215.

- [20] M. Harada and K. Yamayaki, Phys. Repts. 381 (2003) 1.
- [21] R.L. Workman et al. (Particle Data Group), Prog. Theor. Exp. Phys. 2022 (2022) 083C01. <https://pdg.lbl.gov/>
- [22] M. Fujikawa, et al. (Belle Collaboration), Phys. Rev. D 78 (2008) 072006.
- [23] F. Ambrosino, et al. (KLOE Collaboration), Phys. Lett. B 700 (2011) 102.
- [24] M.N. Achasov et al. (SND Collaboration), JETP Lett. 103 (2006) 380.
- [25] J. Gasser and H. Leutwyler, Phys. Rep. 87 (1982) 77.
- [26] H.B. O'Connell, B.C. Pearce, A.W. Thomas, A.G. Williams, Prog. Part. Nucl. Phys. 39 (1997) 201.
- [27] R. Urech, Phys. Lett. B355 (1995) 308.